CHALMERS
UNIVERSITY OF TECHNOLOGY

Cold sprayed Cu/Invar alloy composite

Journal of Materials Research and Technology 34 (2025) 2673–2683

Contents lists available at ScienceDirect

Journal of Materials Research and Technology

journal homepage: www.elsevier.com/locate/jmrt

Cold sprayed Cu/Invar alloy composite

D.L. Ouyang [a,1], Z.R. Wang [a,b,1], T. Yang [a,b], L.W. Zhang [b], D. Wu [b], W.F. Chen [b], Q. Hu [b,*], S. Guo [c]

[a] Key Laboratory for Microstructural Control of Metallic Materials of Jiangxi Province, Nanchang Hangkong University, Nanchang, 330063, China
[b] Institute of Applied Physics, Jiangxi Academy of Sciences, Nanchang, 330096, China
[c] Industrial and Materials Science, Chalmers University of Technology, SE-41296, Göteborg, Sweden

ARTICLE INFO

Handling editor: L Murr

Keywords:
Cold spray
Invar alloy
Thermal conductivity
Thermal expansion coefficient
Electronic packaging materials

ABSTRACT

Cold spray, an additive manufacturing technique based on plastic deformation of particles, was employed to prepare Cu/Invar alloy composites to avoid issues from other preparation methods, like undesirable thermal expansion anisotropy from the extrusion method and the excessive inter-diffusion between Cu and the Invar alloy from the sintering method. For the target $Cu_x(Fe_{64}Ni_{36})_{100-x}$(x = 30–70, wt%) composites prepared by cold spray, the improved thermal expansion anisotropy was reflected by the negligible difference between the thermal expansion coefficient α along and perpendicular to the spray direction, and simultaneously no obvious inter-diffusion was observed between Cu and the Invar alloy $Fe_{64}Ni_{36}$ after annealing at 500 °C. Both α and the thermal conductivity λ increased slightly due to the release of internal stress and recrystallization of Cu. α of the annealed composites basically agreed with the theoretical predication, but λ was far below the values predicted by the Hasselman–Johnson model, mostly because the Invar alloy had an extraordinarily large surface area caused by impact deformation. Even so, the cold-sprayed Cu/Invar alloy composites had clearly advantageous comprehensive performance than those prepared by the traditional sintering and melting methods. Among Cu/Invar alloy composites prepared by different methods, the annealed $Cu_{50}(Fe_{64}Ni_{36})_{50}$ was the only composite having λ larger than 100 W/m•K and isotropic α smaller than 10×10^{-6}/°C. In addition, the cold-sprayed Cu/Invar alloy composites had a good plasticity (after annealing) that is rarely seen in traditional Cu-based composites with high thermal conductivity, presenting a good application potential for electronic packaging materials.

1. Introduction

Electronic packaging materials should ideally have high thermal conductivity λ to quickly conduct heat generated in the semiconductor chip [1], and a low thermal expansion coefficient α matching that of the chip. In addition, weldability and processability are also important, which means the metallic or metal-based materials are preferable candidates [2,3]. Among metallic materials, Cu has a high λ of 397 W/m·K, second only to silver, but a large α of 17×10^{-6}/°C; on the other hand, the $Fe_{64}Ni_{36}$ (wt.%) Invar alloy has the lowest α of 1.2×10^{-6}/°C around room temperature among metallic materials [4,5], but a low λ of 11 W/m·K. Intuitively, Cu/Invar alloy composites could achieve a decent balance between high λ and low α. Fabricating Cu/Invar alloy composites with good comprehensive properties is, however, not an easy task.

The sandwich-structured Cu/Invar alloy/Cu, known as CIC, is the simplest form of Cu/Invar alloy composites [6,7]. It has good heat dissipation in the plane direction but has poor heat conduction in the thickness direction. To address this issue, the powder metallurgy technique was employed to fabricate isotropic Cu/Invar alloy composites [8–13]. The sintering was usually done at 800 °C or higher temperatures, which is essential for densification. The high sintering temperature, however, also accelerated the inter-diffusion between Cu and the Invar alloy. The diffusion of Fe and Ni from the Invar alloy into Cu significantly lowered λ of Cu, while the diffusion of Cu into the Invar alloys on the other hand increased α of the Invar alloy. Applying a silver barrier layer on the Invar alloy powders was employed to reduce the inter-diffusion, but it was not effective [11–13]. As the state of the art, a commercial Cu/Invar alloy composite known as CUVAR® has so far the best comprehensive performance [14]. CUVAR® is produced by several

* Corresponding author.
E-mail address: q-fei618@qq.com (Q. Hu).
[1] These authors are co-first authors of the article.

https://doi.org/10.1016/j.jmrt.2024.12.270
Received 9 November 2024; Received in revised form 30 December 2024; Accepted 31 December 2024
Available online 1 January 2025

steps [15]. Cu and Invar alloy powders are firstly blended according to the composition of $Cu_{43}(Fe_{64}Ni_{36})_{57}$ (wt%), vacuum sealed in a copper tube, heated to about 650 °C, at which temperature the inter-diffusion between Cu and the Invar alloy is negligible, extruded with a reduction ratio of 16:1, and finally annealed at 426–538 °C for about 0.5 h to release the internal stress. The thus produced CUVAR® is fully dense and has a λ of 120 W/m·K, which is better than that of most Cu/Invar alloy composites fabricated by other methods. Unfortunately, the severe elongation of the Invar alloy phase along the extrusion direction results in a 14% lower α in this direction, compared to α in the direction perpendicular to the extrusion direction. The anisotropy of α would result in thermal stress during thermocycling and thus pose a risk of device failure.

Two challenges for improvements are identified from the descriptions above. First, densification needs to be done at temperatures below 800 °C, using techniques other than high temperature sintering, to prevent undesirable inter-diffusion between Cu and the Invar alloy. Second, elongation of the Invar alloy phase along a specific direction should be avoided, which means extrusion and rolling are out of consideration. Cold spray [16–18], an additive manufacturing based on the local plastic deformation of particles, is a feasible way to tackle both challenges. The particles are accelerated by high-pressure inert gas through a Laval nozzle and then deposited on a substrate. The deposition mechanism is based on severe plastic deformation of particles induced by high-speed impact, which is significantly different with particles being melted as in the case of thermal spray. The term "cold" essentially means the particles are solid, rather than liquid, before deposition. Indeed, the particles are usually heated, by hot inert gas, to achieve better plasticity. Compared to thermal spray, cold spray has several advantages, including little increase in the oxygen content, minimum temperature increase during deposition and thus little diffusion or phase transition, and high deposition speed and thus easy fabrication of bulk samples with a large volume or a large area. Both Cu and Invar alloys have good plasticity, due to their face centered cubic (fcc) structure, and they are suitable for cold spray. Indeed, the cold sprayed Cu and Invar alloys already exhibited high thermal conductivity [19] and low thermal expansion coefficient [20], respectively. Therefore, it is expected that cold sprayed Cu/Invar alloy composites could have a decent balance of high thermal conductivity and low thermal expansion coefficient, which motivates the current work.

2. Experimental details

Cu and $Fe_{64}Ni_{36}$ powders were first blended according to the compositions of $Cu_x(Fe_{64}Ni_{36})_{100-x}$(x = 20, 30, 40, 50, 60, 70, wt%), and then sprayed using the parameters list in Table 1. The deposited materials, with a dimension of 100 × 70 × (8–10) mm^3, were removed from the Al substrate and then cut into small pieces with a dimension of 10 × 10 × 2 mm^3 along the horizontal cross-section and 10 × 8 × 2 mm^3 along the vertical cross-section. The small piece samples were vacuum sealed in quartz tubes and annealed at 500 °C for 3 h and 950 °C for 3 h, respectively. The microstructure and phase constitution of as-sprayed and annealed samples were analyzed by optical microscope (OM, LEICA DMI 3000 M), scanning electron microscope (SEM, ZEISS EVO 18) and X-ray diffractometer (XRD, Bruker D8 Advance, 40KV × 200 mA), respectively. The X-ray computed tomography (XCT, ZEISS XRADIA 620 VERSA, 140KV × 150 μA) with a spatial resolution of 0.9975 μm was employed to analyze the inner microstructure of an as-sprayed $Cu_{50}(Fe_{64}Ni_{36})_{50}$ (Cu50 for short) sample with a dimension of Φ1.2 mm × 5 mm. α was measured by dilatometer (NETZSCH DIL 402C) using a heating rate of 5K/min and a load of 200 mN. λ at room temperature was determined using the formula $\lambda = \rho \times D \times C$, where the density ρ was measured using the Archimedes method, and the thermal diffusivity D and the specific heat capacity C were measured using a laser flash thermal conductivity measurement apparatus (NETZSCH LFA457). Tensile tests were carried out on the Cu50 sample using a universal testing machine (MTS, CMT5205) with an initial strain rate of 1×10^{-3}/s.

3. Results and discussion

3.1. Microstructure

Fig. 1 shows that the raw Cu and Invar alloy powders had a good degree of sphericity and narrow particle size distribution. D_{50} of Cu and Invar alloy powders were 37.6 and 36.7 μm respectively, which are suitable particle sizes for cold spray. The deposited materials showed color change with varying compositions but all of them showed no sign of visible oxidation, which is an advantage of cold spray.

The backscattered electron (BSE) images in Fig. 2 show that the dark Invar alloy phase and the light Cu phase were uniformly distributed, and the shape of two phases were in stark contrast with the initial spherical form shown in Fig. 1. When a high-speed powder impacts on the substate, the large impact force results in a crowding-out effect of the powder, which was widely verified by extensive observations in single powder cold spray [21–23]. As indicated by the schematic in Fig. 3, when an Invar alloy powder and a Cu powder impact on the substrate in succession, the Invar alloy particles firstly change to a hat shape due to the crowding-out effect, and then to a bowl shape upon further impact compression from the Cu particles; when two Invar alloy powders impact in succession, a thick hat shape forms. The perfect bowl and thick hat shape of the Invar alloy particles occur only when two particles (Invar alloy/Cu or Invar alloy/Invar alloy) impact on the same spot. If not, as is the more common case, various shapes would occur, as shown in Fig. 2. On the other hand, since Cu is softer than the Invar alloy, the Cu particles experience more deformation, hence displaying more irregular shapes as seen in Fig. 2.

The severe impact deformation significantly changes the shape of raw particles and their surface area. The surface area change, however, can hardly be investigated by SEM. In addition, it is also difficult to distinguish whether the many black holes in the BSE images are formed during deposition or during sample preparation, since some loose particles may fall off during polishing. The XCT technique, which can detect the inner three-dimensional information of the bulk sample [24], was thus employed to carefully investigate the two phases, i.e., Cu and the Invar alloy, and the holes. The X-ray is dampened differently when passing through different materials, which mostly depends on the density and the damping factor of the materials. The transmission X-ray forms a projection at the detector behind the sample. With the sample rotation, multiple projections are gained and assembled to formulate a three-dimensional graph through a CT algorithm. On the other hand, slices along the radial and axial directions of the cylinder sample can be obtained by disassembling the three-dimensional graph.

As shown in the XCT slices in Fig. 4, the black, dark and lighter regions are holes, the Invar alloy and Cu, respectively, which is similar to the BSE images shown in Fig. 2. The difference is that it is affirmed now

Table 1
Cold spray process parameters (PSC-1000L, Japan Plasma Technology Research Industry Co. Ltd).

Powders	Substrate	Gas	Pressure	Chamber Temperature	Sprayed Distance	Gun Speed
Cu + $Fe_{64}Ni_{36}$	Al	N_2	5 MPa	700 °C	20 mm	200 mm/s

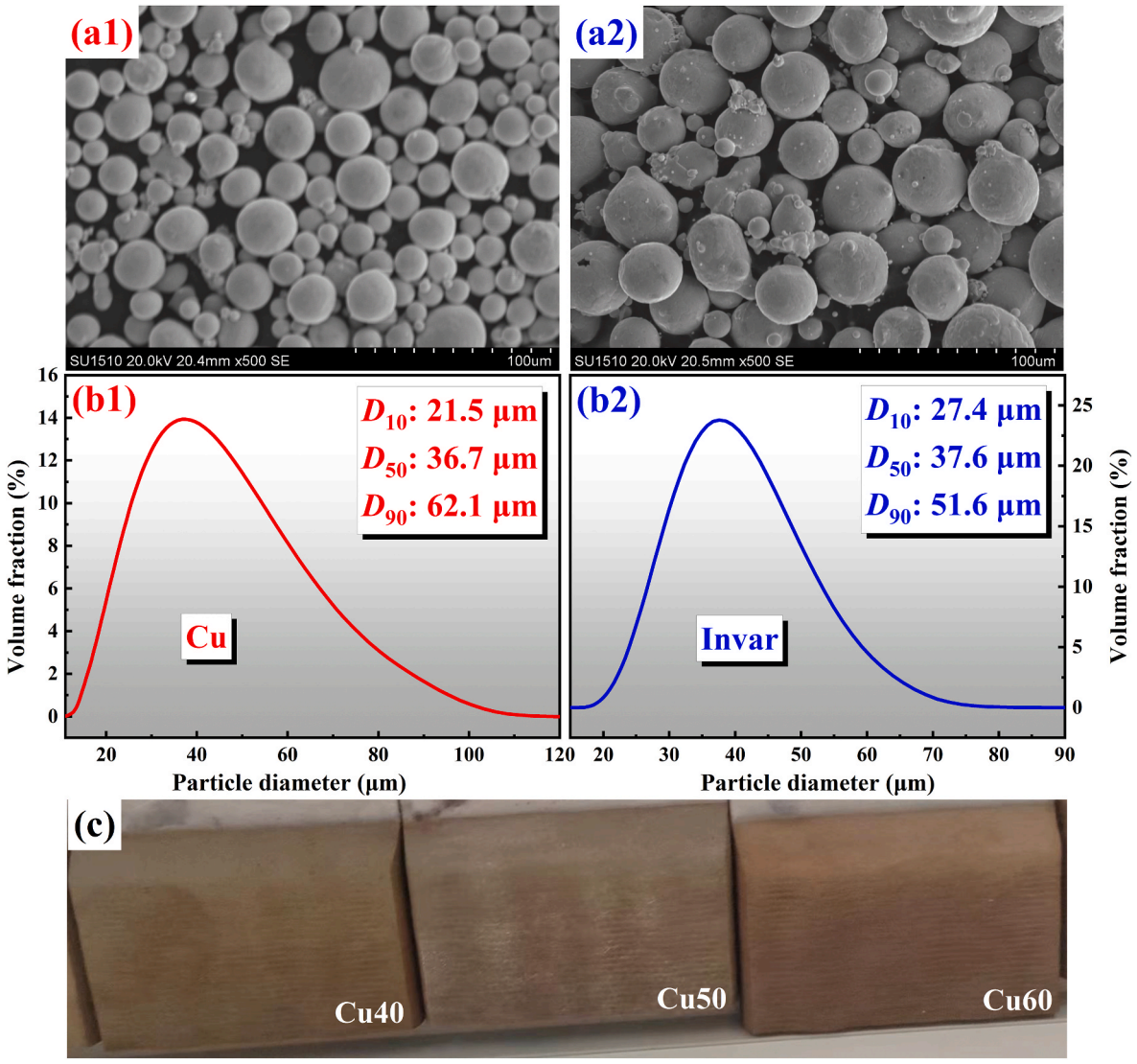

Fig. 1. (a1, a2) SEM images and (b1, b2) particle size distributions of the raw Cu and Invar alloy powders, and (c) the appearance of the cold sprayed Cu/Invar alloy composites.

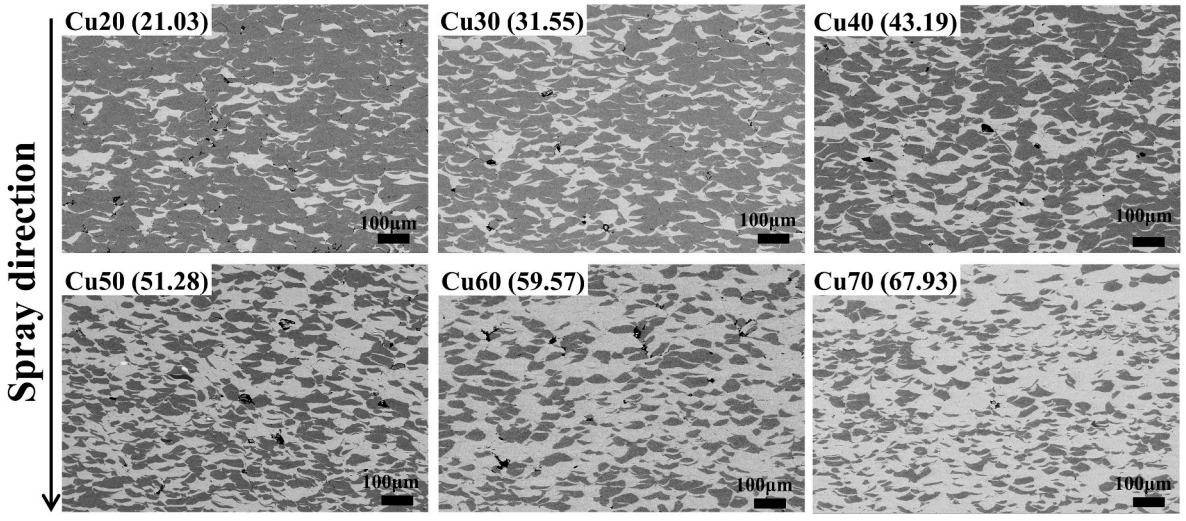

Fig. 2. BSE images of the cold-sprayed $Cu_x(Fe_{64}Ni_{36})_{100-x}$ composites. The measured x values are indicated in the brackets.

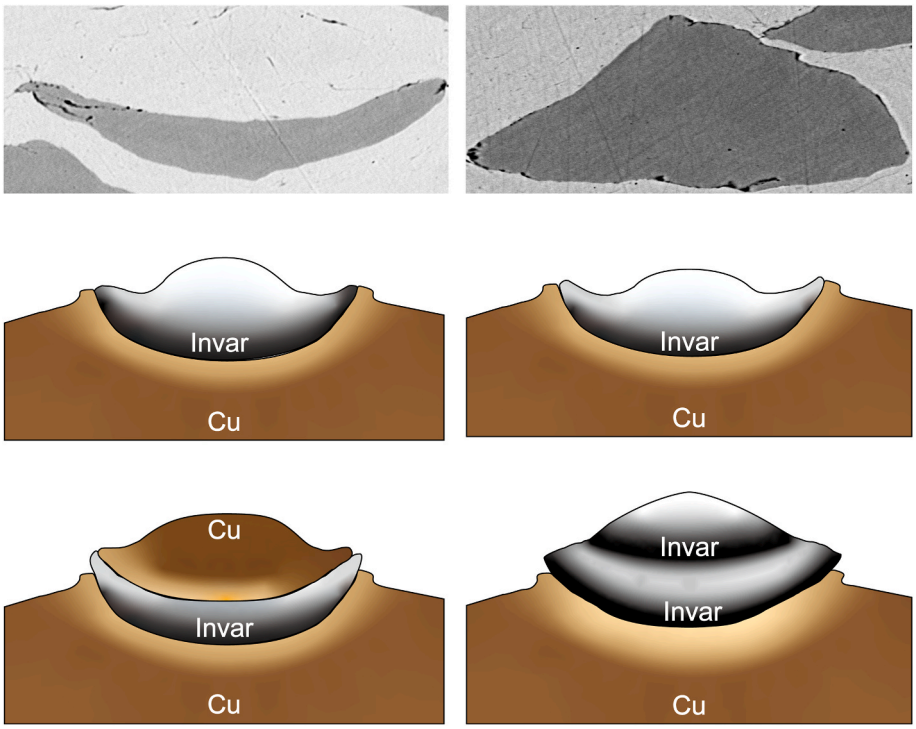

Fig. 3. Schematic of the deformation of the Invar alloy particles.

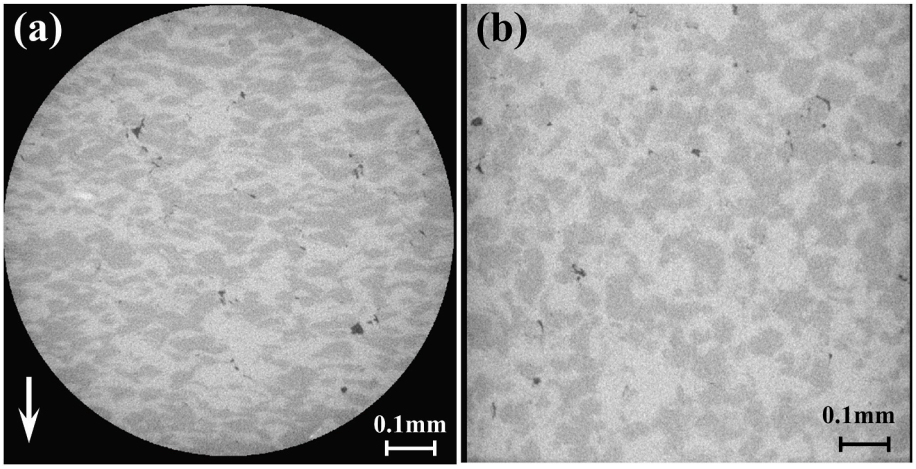

Fig. 4. XCT slices along the (a) radial and (b) axial directions in the Cu50 composite. The arrow of (a) denotes the spray direction.

that these holes were formed during deposition. The total volume fraction of the holes is 0.12%. If there is only one spherical hole with the same volume fraction in a 1-g composite, the surface area of this hole is 1.3 mm^2. However, there were 201 small holes in the detected region as shown in Fig. 5(c), corresponding to 102550 holes in a 1-g composite. The detected total specific surface area for the holes thus dramatically increased to 147 mm^2/g, as listed in Table 2.

More importantly, Cu and the Invar alloy also had extraordinarily large surface areas of 50465 and 76472 mm^2/g respectively, which was attributed to two factors. One is that the raw particles already had large surface areas. As a comparation, the raw powders of the CUVAR® composite had diameter about an order of magnitude larger, and thus had surface area about an order of magnitude smaller, as listed in Table 2. The other is that the severe impact deformation made the surface areas of the particles increase about 4~6 times, larger than the increase of 1~2 times for the particles in CUVAR®, as listed in Table 2. The large surface areas of the Invar alloy phase in the cold sprayed composite lowered the thermal conductivity significantly, which will be discussed later.

3.2. Thermal expansion behavior

The cold sprayed Cu/Invar alloy composites were formed by plastic deformation of particles, with a similar but different forming mechanism of CUVAR®. α was thus carefully examined along the vertical cross-section and horizontal cross-section, to check if anisotropy of thermal expansion also existed in the cold sprayed materials. The average α value in the temperature range of 20~100 °C, $\alpha_{20\text{-}100}$, which is an important parameter for electronic packaging materials [3], were measured along two orientations. As shown in Figs. 6 and 7, most composites had a close $\alpha_{20\text{-}100}$ along two orientations, with a difference of 0.04–0.16 × 10^{-6}/°C that was negligible when considering the measurement error. However,

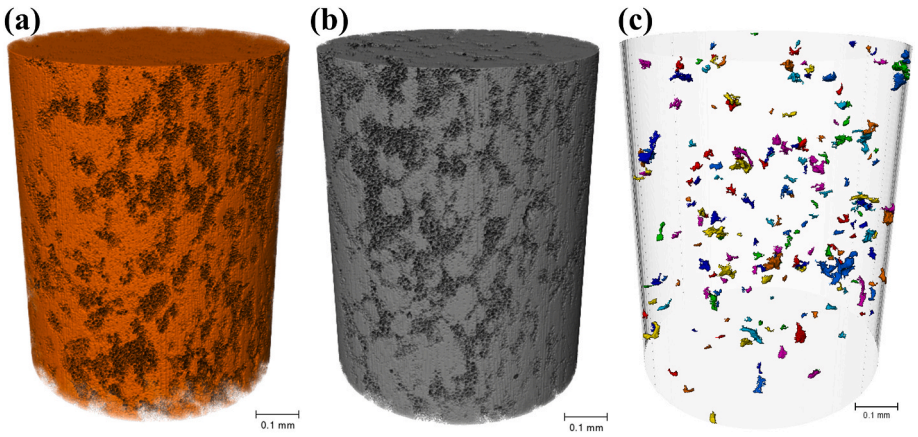

Fig. 5. 3D XCT graphics of (a) the Invar alloy, (b) Cu, and (c) holes in the as-sprayed Cu50 composite.

Table 2
The volume and surface area of Cu, the Invar alloy phase, and holes in two Cu/Invar alloy composites.

Materials		Phase	Mass fraction	Volume fraction	Particle diameter (μm)	Specific surface area (mm^2/g)①
CUVAR®	Raw particles	Cu	41.7%	40%	300	937
		Invar	58.3%	60%	300	1439
	Composite	Cu	41.7%	40%	N/A	2080~3491②
		Invar	58.3%	60%	N/A	3122~5237②
		Holes	N/A	0	N/A	0
Cu50	Raw particles	Cu	49.4%	47.70%	36.7	9074
		Invar	50.6%	52.30%	37.6	9968
	Composite	Cu	49.4%	47.64%	N/A	50465
		Invar	50.6%	52.24%	N/A	76472
		Holes	N/A	0.12%	N/A	147

Note.
①: Calculated based on 1 g composite.
②: Assuming a spherical powder with a diameter d ($d = 300$ μm) is extruded to a cylinder with a length l ($l = 1726$–6026 μm) and a radius r ($r = 51$~27 μm), where $\ln(l/d) = 1.75$–3 [15].

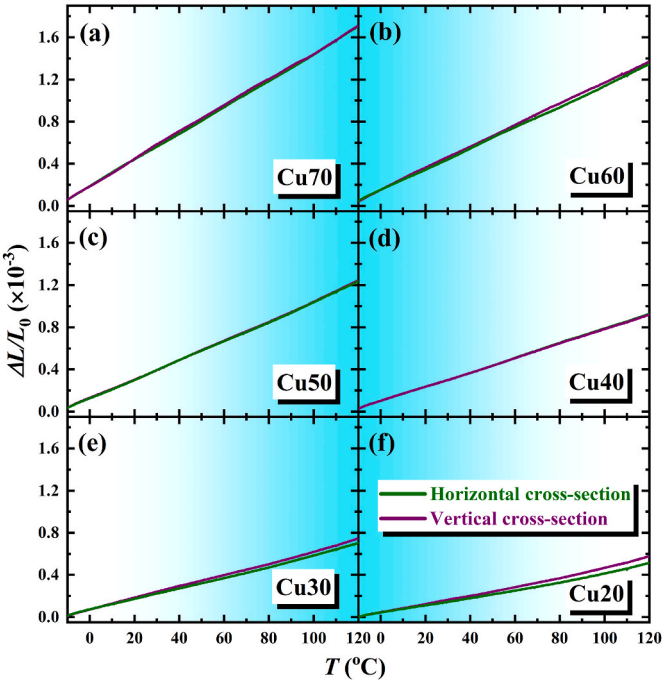

Fig. 6. Thermal dilation traces along the vertical cross-section and horizontal cross-section.

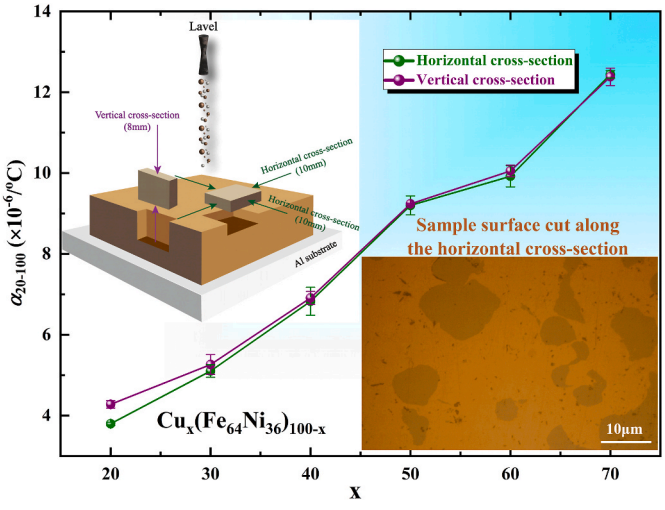

Fig. 7. $\alpha_{20\text{-}100}$ of the as-sprayed Cu/Invar alloy composites. The insets show the schematic of sample cutting, and an OM image of the sample surface cut along the horizontal cross-section.

for Cu20 containing 80 wt% of the Invar alloy phase, $\alpha_{20\text{-}100}$ measured along the horizontal cross-section was 0.5×10^{-6}/°C lower than that measured along the vertical cross-section, which could not be ignored. The Invar alloy phase was compressed along the vertical cross-section and stretched along the horizontal cross-section, as shown in Figs. 2 and 3, which resulted in a higher proportion of the Invar alloy phase and

thus a lower α along the horizontal cross-section [14]. The difference in α between two orientations depends on the amount, shape and orientation of the Invar alloy phase. For the cold sprayed composites, the Invar alloy phase stretched along the horizontal cross-section but without preferred orientation, as shown by the OM image in Fig. 6. For CUVAR®, however, under the large true strain of 1.75–3, the spherical Invar alloy particles were extruded into a cylinder shape along the extrusion direction [14], showing much stronger preferred orientation than cold sprayed composites. Therefore, for CUVAR®, the difference in α between the longitudinal direction (i.e., extrusion direction) and transverse direction was as large as 1.0×10^{-6}/°C, even though the weight percentage of the Invar alloy phase was only 57%. By contrast, for cold sprayed composites, even when the weight percentage of the Invar alloy phase reached 80%, a mere difference of 0.5×10^{-6}/°C between two orientations was seen. Other composites containing lower weight percentages of the Invar alloy phase could be deemed isotropic in terms of thermal expansion, and in the following text $\alpha_{20\text{-}100}$ values measured along the horizontal cross-section were used.

3.3. The effect of annealing

Cold sprayed composites usually have a large internal stress due to severe plastic deformation of particles. Annealing is necessary to eliminate internal stress but has the possibility to also change the structure and property of the composites. As shown in Figs. 8 and 9(a), after annealing at 500 °C for 3 h, all composites had a slight increase in α, due to the release of internal stress that otherwise could restrict the thermal expansion to some extent [25]. Actually, the cold spray pure Invar alloy has a negative α if the compressive residual stress is large enough [20]. Fig. 9(b) shows that, after annealing at 500 °C for 3 h, Cu60 and Cu70 had a rather large increase in λ, while other composites had a marginal increase in λ. This phenomenon was mostly attributed to the morphology change of Cu after annealing. Due to the high strain rate up to 10^6~10^9/s induced by the high velocity impact [26,27], the Cu grains broke into smaller pieces, as shown in Fig. 10(a). After annealing, the recrystallized Cu grains grew to formulate large and regular grains, as shown in Fig. 10(b). More importantly, the interface between particles in the as-sprayed sample, as indicated by the arrows in Fig. 10(a), disappeared. Thus, the Cu phase could be deemed as a continuous matrix. Large grains with less grain boundaries are beneficial for the heat conduction [28], and this effect is even more significant when there is a higher volume percentage (>50 wt%) of the Cu phase. Therefore, Cu60 and Cu70 had a more significant increase in λ than other composites.

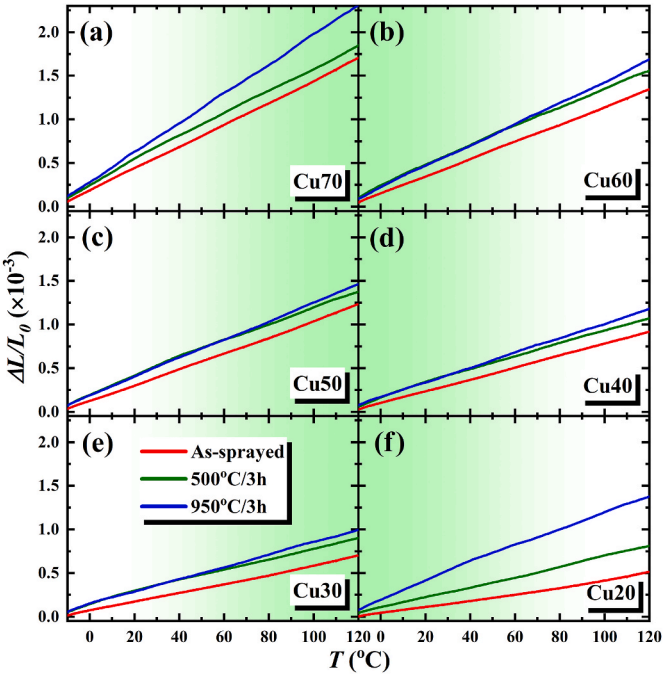

Fig. 8. Thermal dilation traces of as-sprayed and annealed composites.

Annealing at 500 °C for 3 h did not change the compositions of each phase, since the EDS line scanning results shown in Fig. 11 were almost identical to those in the as-sprayed condition, and the XRD patterns shown in Fig. 12 also did not change much. Annealing at 950 °C for 3 h, however, caused a clear inter-diffusion among the three elements. For Cu50, the concentration of Cu is higher than that of Fe and Ni, hence the diffusion of Cu into the Invar alloy phase was more severe than that of Fe and Ni into the Cu phase, as shown in Fig. 11. The diffusion made the diffraction peaks of Cu and the Invar alloy phase, both having a fcc structure, merge into one peak, as shown in Fig. 12. The atomic radius of Fe, Ni and Cu is 1.241, 1.246 and 1.278 Å, respectively. The diffusion of Fe and Ni into the Cu phase thus resulted in a lattice shrinkage, manifested by a right shift of the diffraction peak. The heterogenous atomic occupancy in the Cu lattice resulted in additional scattering and hence significantly lowered λ [13]. On the other hand, the inter-diffusion changed the composition of the Invar alloy phase, by increasing the Cu content and decreasing the Fe and Ni contents, and thus was harmful to the low thermal expansion characteristic. Consequently, after annealing at 950 °C for 3 h, there was a noticeable increase in α.

The mechanical properties also changed sharply after annealing. As shown in Figs. 13 and 14, the as-sprayed Cu50 had a high hardness, both in the Cu phase and the Invar phase, but a very low strength of 156 MPa without yielding in the tension test. Similar phenomenon, i.e., hard but brittle behavior was also found in the cold-sprayed pure Cu [29], and it was mostly attributed to the internal stress. The internal stress was generated from the mismatch of plastic deformation between Cu and the Invar phase. During deposition, the Cu phase underwent a more severe plastic deformation than the Invar phase, which can be deduced from two observations. One is the more irregular shapes of the Cu phase shown in the BSE photos of Fig. 2. The other is the hardness of the Cu phase decreased by about a half, while that of Invar phases only decreased by about one-third after annealing, which means the Cu phase was more deformed in the as-sprayed state. On the other hand, the strength and plasticity increased significantly after annealing. The tensile elongation of the annealed Cu50 was 15%, which was much inferior to the value of 40% of the cold-sprayed Cu after being annealed at 500°C for 4 h [30], but was rather close to the value of 21% of the cold-sprayed Invar alloy after being annealed at 800°C for 3 h [20]. The ultimate tensile strength of annealed Cu50 was 428 MPa, which was, again, much larger than 250 MPa of the cold-sprayed and annealed Cu [30], and close to 472 MPa of the cold-sprayed and annealed Invar alloy [20]. These phenomena indicated that the mechanical property of the annealed Cu50 is dominated by the Invar phase, which acts as the reinforcement phase and has a volume fraction larger than 50%.

3.4. Theoretical models for α and λ

After annealing at 500 °C for 3 h, there still had two distinct phases without significant inter-diffusion; the internal stress was released; the Cu particle boundaries were eliminated by recrystallization and a continuous Cu matrix formed. The Cu/Invar alloys composites were thus in a stable state and how the properties, i.e., $\alpha_{20\text{-}100}$ and λ, change with the compositions can now be investigated. There are several theoretical models proposed to describe the thermal expansion of the composites [31–34]. The simplest one is the rule-of-mixture (ROM) model [34], given by

$$\alpha_c = \alpha_m V_m + \alpha_p V_p \quad (1)$$

where α and V are the thermal expansion coefficient and volume fraction, respectively, and subscripts c, m and p denote composite, matrix

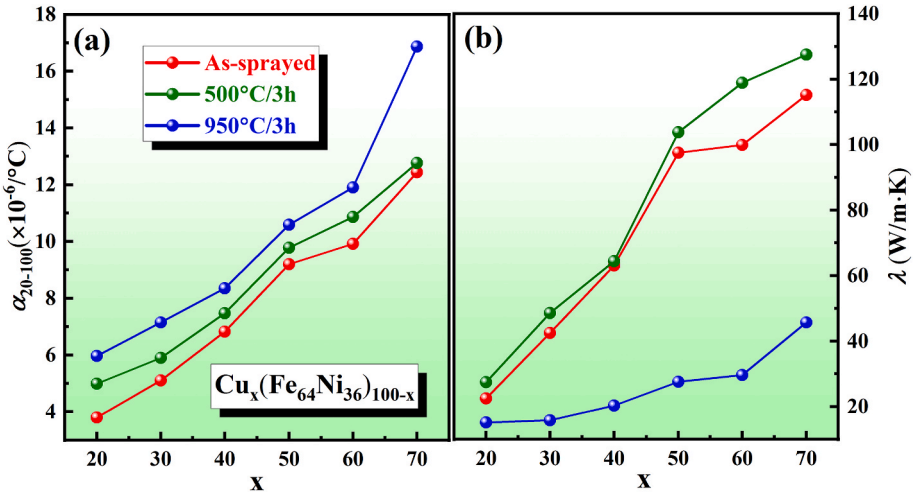

Fig. 9. (a) α and (b) λ of as-sprayed and annealed composites.

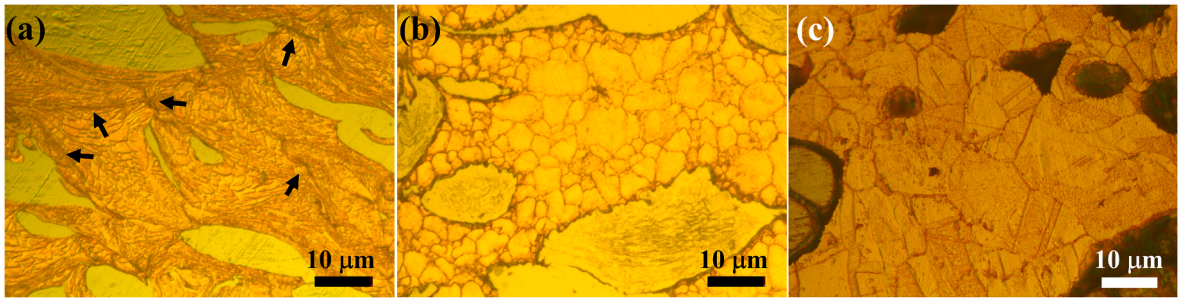

Fig. 10. OM images of as-sprayed and annealed Cu50.

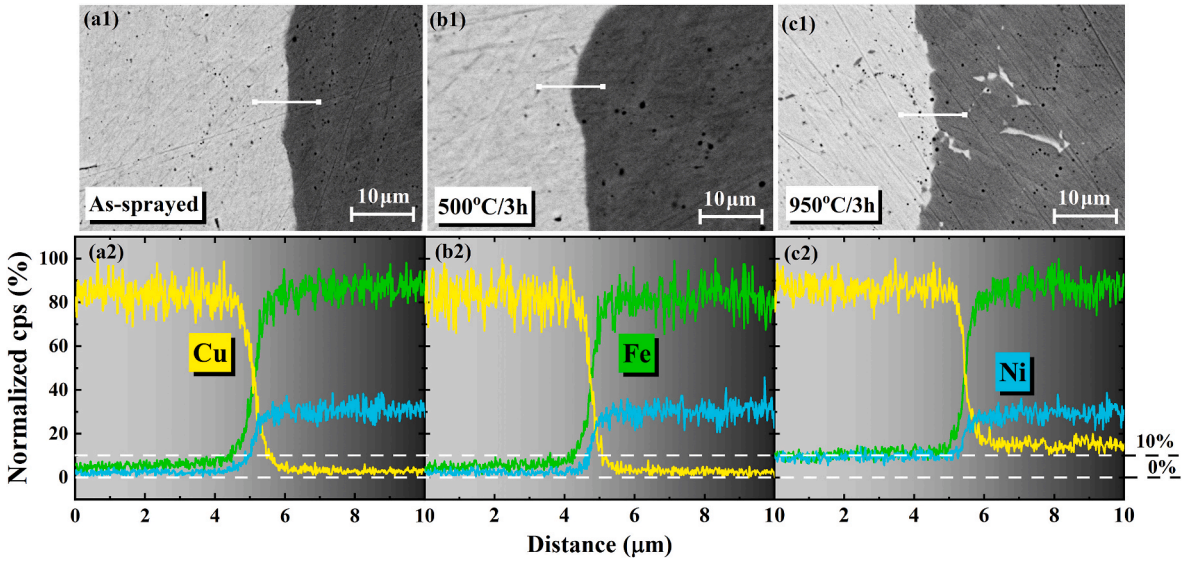

Fig. 11. EDS line scanning results of Cu50 in as-sprayed and annealed conditions.

(Cu) and secondary phase (Invar alloy), respectively. Effects of several factors on the thermal expansion are not taken into consideration in the ROM model, such as the holes, internal stress, elastic modulus difference between two phases, the shape of the secondary phase, etc. This simplest model, however, still works reasonably well as shown in Fig. 15(a), indicating that these factors do not have a significant effect on the thermal expansion, at least for the cold sprayed Cu/Invar alloy composites.

For λ, the Hasselman–Johnson (H–J) model [35] is a sophisticated one since in addition to the volume fraction of the secondary phase, the particle size and the interfacial thermal resistance (ITR) are also taken into consideration. It is expressed by

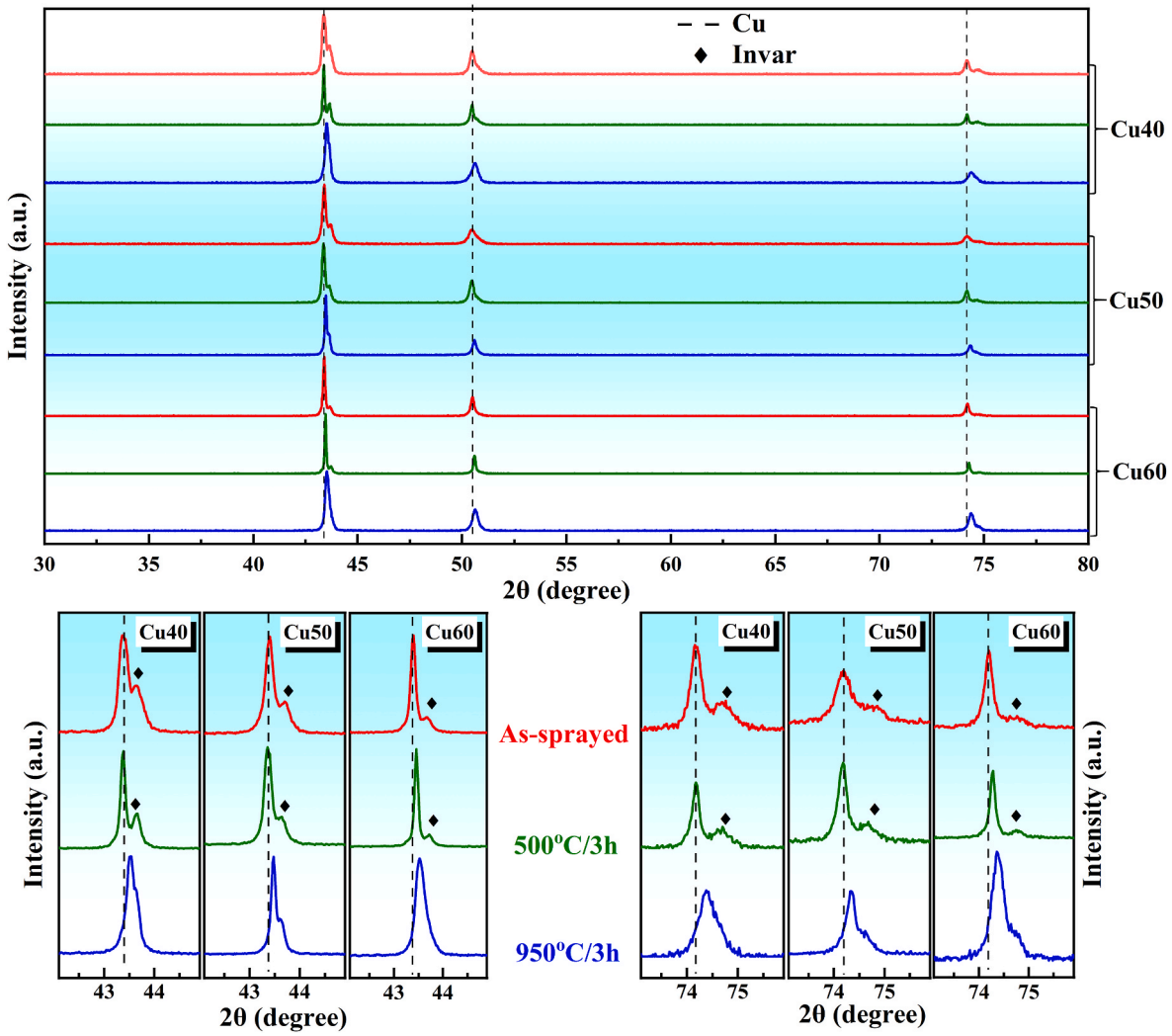

Fig. 12. XRD patterns of three composites in as-sprayed and annealed conditions.

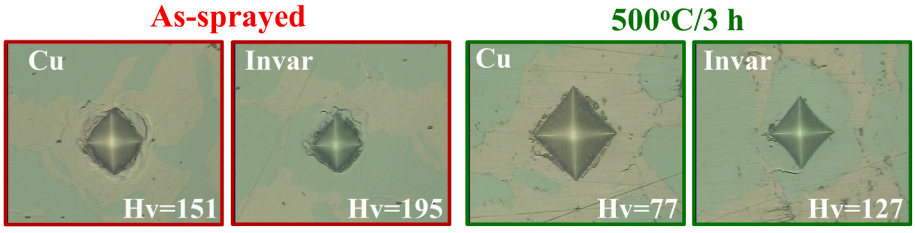

Fig. 13. Hardness of Cu and the Invar phase in as-sprayed and annealed conditions.

$$\lambda_c = \lambda_m \frac{[\lambda_p(1+2\beta)+2\lambda_m]+2V_p[\lambda_p(1-\beta)-\lambda_m]}{[\lambda_p(1+2\beta)+2\lambda_m]-V_p[\lambda_p(1-\beta)-\lambda_m]} \quad (2)$$

where λ and V are the thermal conductivity and volume fraction, respectively, and subscripts c, m and p denote composite, matrix (Cu) and secondary phase (Invar alloy), respectively. The non-dimensional parameter β is defined as

$$\beta = R_{ITR} \cdot \lambda_m / d \quad (3)$$

where R_{ITR} and d are the specific ITR and the radius of the secondary phase particles, respectively. When the ITR is very small, i.e., $R_{ITR} \to 0$ and thus $\beta \to 0$, Eq (2) is simplified to

$$\lambda_c = \lambda_m \frac{(\lambda_p+2\lambda_m)-2V_p(\lambda_m-\lambda_p)}{(\lambda_p+2\lambda_m)+V_p(\lambda_m-\lambda_p)} \quad (4)$$

which is the Maxwell model [36,37], the simplest and well-known model for the thermal conductivity of composites. On the contrary, when the ITR is very large, i.e., $R_{ITR} \to \infty$ and thus $\beta \to \infty$, Eq (2) is simplified to

$$\lambda_c = 2\lambda_m \frac{1-V_p}{2+V_p} \quad (5)$$

All possible λ predicated by H-J model are included in a narrow region surrounded by two lines calculated based on Eqs. (4) and (5). The measured λ, however, are far below this theoretically predicted region.

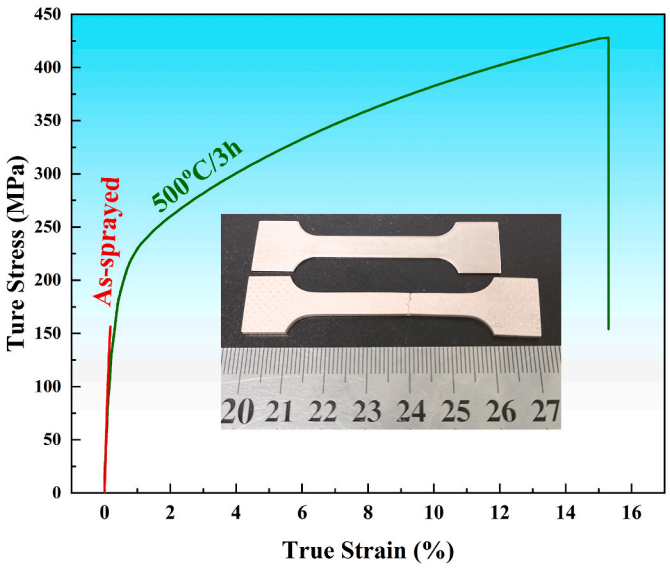

Fig. 14. Tensile test results of as-sprayed and annealed Cu50. The inset photo shows the comparison of the untested sample and the annealed sample after failure.

The failure of the H-J model is mostly attributed to the underestimation of the total ITR. The total ITR depends on the physical property of the interface, i.e., the R_{ITR}, and the total interfacial area. The H-J model is built based on a presumption of secondary phase in the form of spherical particles that are commonly seen in the powder metallurgy prepared composites [38]. In the H-J model, the total interfacial area only depends on the volume fraction V_p and the radius d of the secondary phase. In cold sprayed composites, however, the Invar alloy phase had the bowl, hat and other shapes due to the severe plastic deformation, as shown in Figs. 2 and 3. The surface area of the Invar alloy phase increased about 4~6 times when comparing to that of the raw spherical powders, as indicated by Table 2. Therefore, even at the limit of $R_{ITR}\rightarrow\infty$, the H-J model is unlikely to be accurate because only a small part of interface is counted in the model. Indeed, the distance between two lines calculated at the limits of $R_{ITR}\rightarrow 0$ and $R_{ITR}\rightarrow\infty$ is small, which indicates that the role of ITR is insignificant in the H-J model, at least for the Cu/Invar alloy composites. In addition, another presumption of the H-J model is the fully dense composite without any holes. As listed in Table 2, although holes had a volume fraction of only 0.12%, they had a rather large surface area, increasing more than 100 times when compared to a single spherical hole with the same volume. These holes have a large R_{ITR} and thus a non-negligible contribution to the total ITR, even though the total surface area of the holes is incomparable to that of the Invar alloy phase. In short, a theoretical model that can accurately describe the thermal conductivity of cold sprayed Cu/Invar alloy composites is still lacking and further investigations are warranted.

3.5. Comprehensive properties

Fig. 16 summarizes α and λ of existing Cu/Invar alloy composites prepared by different methods [8–14,39,40]. Pure Cu and the Invar alloy are connected by a theoretical line based on the simplest ROM and Maxwell models. Among dozens of Cu/Invar alloy composites, there is only one data point, i.e., CUVAR® along the longitude direction, falls on this theoretical line, indicating a challenging task for fabricating Cu/Invar alloy composite with theoretical α and λ. Another data point of CUVAR® along the transverse direction has α 1×10^{-6}/°C higher. The α value of the cold sprayed Cu40, with a similar composition to CUVAR®, is 7.5×10^{-6}/°C, just between those of CUVAR® along two directions. Its λ of 64 W/m·K, however, is much inferior to 120 W/m·K of CUVAR®, mostly because the much larger surface area of the Invar alloy phase of the cold sprayed composite. Even so, the cold sprayed Cu/Invar alloy composites have clearly better comprehensive properties than those prepared by other methods including sintering and melting, mostly because the lower temperature needed by cold spray, as indicated by the legend of Fig. 16. For sintering, it is difficult to solve the conflict between high density and low inter-diffusion, since high pressure and high temperature are required by the former which are however harmful to the latter. Strictly speaking, the product of arc melting is not a composite, but an alloy containing Cu-rich and Invar alloy-rich phases [40], which results in low λ, as shown in the bottom part of Fig. 16.

With the increasing power consumption of the chip, the minimum requirements for the heat sink are λ larger than 100 W/m·K and α lower than 10.0×10^{-6}/°C. The cold sprayed Cu50 after annealing at 500 °C

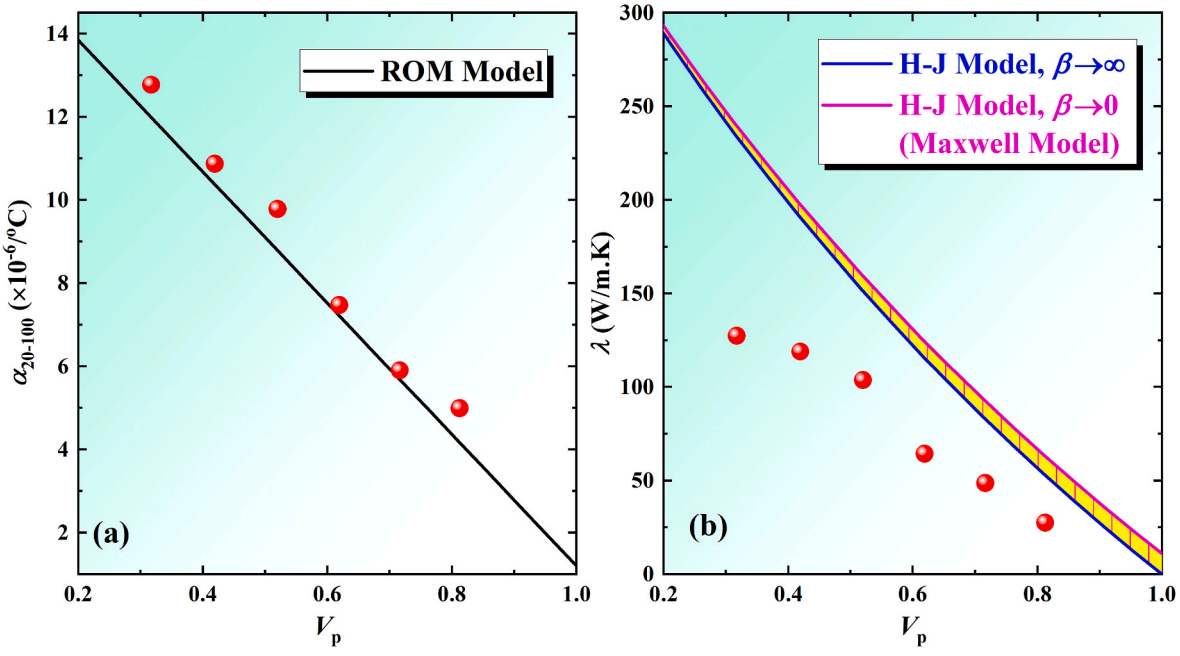

Fig. 15. Agreements between theoretical model predictions for α and λ and experimental measured values.

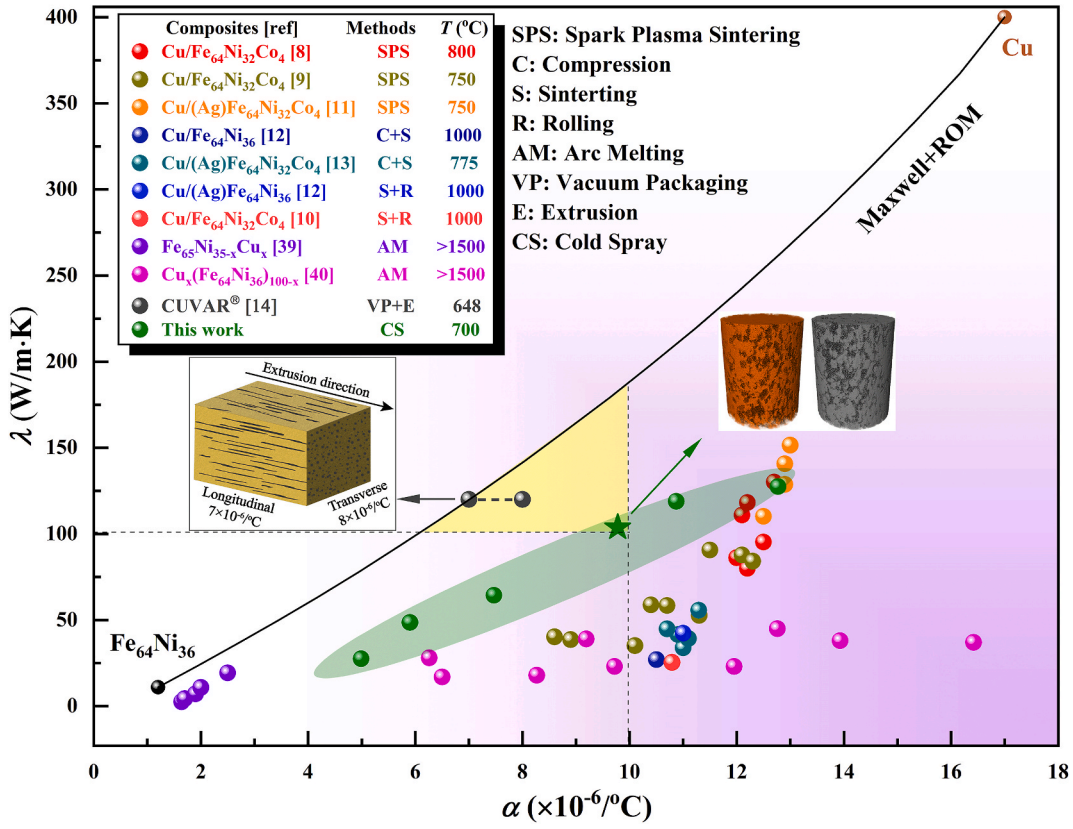

Fig. 16. α and λ of Cu/Invar alloy composites prepared by different methods.

for 3 h had λ of 104 W/m·K and α of 9.2 × 10^{-6}/°C, which is the only Cu/Invar alloy composite meeting these two requirements, if not considering CUVAR® which shows anisotropic α that would lead to thermal stress. λ could be further optimized by adjusting the cold spray technique, such as using larger Invar alloy powders to reduce the surface area, but are still much inferior to that of Cu/SiC [41], Cu/Diamond [42], Cu/W [43] and Cu/Mo [44] composites, due to the innate low λ of 11 W/m·K of the Invar alloy. However, the processability of Cu/Invar alloy composites, which is guaranteed by the good plasticity shown in Fig. 14, is much better than those Cu-based composites containing a hard secondary phase. In addition, a large volume or area of Cu/Invar alloy composites can be easily fabricated by cold spray, which is a unique advantage over other Cu-based composites. These features make the cold sprayed Cu/Invar alloy composites potentially useful in some special field, such as the cooling backboard of the large flat panel display.

4. Conclusions

In conclusion, two major issues of Cu/Invar alloy composites fabricated by traditional methods, i.e., anisotropic thermal expansion by the extrusion method, and the high temperature inter-diffusion between Cu and the Invar alloy by the sintering method, were tackled by using the cold spray method. A new problem, however, appeared in that the large surface area of the Invar alloy, introduced by impact deformation, resulted in a large interfacial thermal resistance and thus lowered the thermal conductivity significantly. Even so, among existing Cu/Invar alloy composites prepared by different methods, the annealed $Cu_{50}(Fe_{64}Ni_{36})_{50}$ composite was the only material meeting requirements of λ larger than 100 W/m•K and isotropic α smaller than 10 × 10^{-6}/°C. Together with the unique advantage of good processability, the cold sprayed Cu/Invar composites present a high application potential in the domain of electronic packaging materials.

Declaration of competing interest

The authors declare that they have no known competing financial interests or personal relationships that could have appeared to influence the work reported in this paper.

Acknowledgments

The authors acknowledge financial support from the National Natural Science Foundation of China (NSFC, Nos. 52061016and 52461024), the Major Scientific and Technological R&D Projects of Jiangxi Province (No. 20212AAE01003), the Special International Cooperation Project of Jiangxi Province (No. 20232BBH80008), the Natural Science Foundation of Jiangxi Province (No.20242BAB25216), and the internal funding from the Jiangxi Academy of Sciences (Nos. 2022YSBG10001 and 2023YSBG21013).

References

[1] Garimella SV, Fleischer AS, Murthy JY, Keshavarzi A, Prasher R, Patel C, et al. Thermal challenges in next-generation electronic systems. IEEE Trans Compon Packag Technol 2008;31:801–15. https://doi.org/10.1109/tcapt.2008.2001197.
[2] Baig MMA, Hassan SF, Saheb N, Patel F. Metal matrix composite in heat sink application: reinforcement, processing, and properties. Materials 2021;14:6257. https://doi.org/10.3390/ma14216257.
[3] Qu XH, Zhang L, Wu M, Ren SB. Review of metal matrix composites with high thermal conductivity for thermal management applications. Prog Nat Sci: Mater Int 2011;21:189–97. https://doi.org/10.1016/s1002-0071(12)60029-x.
[4] Guillaume CE. Invar and its applications. Nature 1904;71:245. https://doi.org/10.1038/071134a0.
[5] van Schilfgaarde M, Abrikosov IA, Johansson B. Origin of the Invar effect in iron-nickel alloys. Nature 1999;400:46–9. https://doi.org/10.1038/21848.
[6] Chen P, Huang HG, Ji C, Zhang X, Sun ZH. Bonding strength of Invar/Cu clad strips fabricated by twin-roll casting process. Trans Nonferrous Metals Soc China 2018; 28:2460–9. https://doi.org/10.1016/s1003-6326(18)64892-7.
[7] Ji C, Huang HG, Zhang X, Zhao RD. Numerical and experimental Research on fluid flow, solidification, and bonding strength during the twin-roll casting of Cu/invar/

Cu clad strips. Metall Mater Trans B 2020;51:1617–31. https://doi.org/10.1007/s11663-020-01854-4.
[8] Nie QQ, Chen GH, Wang B, Yang L, Zhang JH, Tang WM. Effect of Invar particle size on microstructures and properties of the Cu/Invar bi-metal matrix composites fabricated by SPS. J Alloys Compd 2022;891:162055. https://doi.org/10.1016/j.jallcom.2021.162055.
[9] Nie QQ, Chen GH, Wang B, Yang L, Tang WM. Process optimization, microstructures and mechanical/thermal properties of Cu/Invar bi-metal matrix composites fabricated by spark plasma sintering. Trans Nonferrous Metals Soc China 2021;31:3050–62. https://doi.org/10.1016/s1003-6326(21)65714-x.
[10] Wu D, Yang L, Shi CD, Wu YC, Tang WM. Effects of rolling and annealing on microstructures and properties of Cu/Invar electronic packaging composites prepared by powder metallurgy. Trans Nonferrous Metals Soc China 2015;25:1995–2002. https://doi.org/10.1016/s1003-6326(15)63808-0.
[11] Nie QQ, Wang B, Zhang JH, Tang WM. Fabrication of the Ag-coated Invar/Cu bimetal matrix composites through spark plasma sintering: an investigation on microstructure and properties. Mater Lett 2022;321:132440. https://doi.org/10.1016/j.matlet.2022.132440.
[12] Zhang X, Wu D, Yang L, Shi CD, Wu YC, Tang WM. Microstructures and properties of Cu/Ag(Invar) composites fabricated by powder metallurgy. Trans Nonferrous Metals Soc China 2017;27:1759–66. https://doi.org/10.1016/s1003-6326(17)60198-5.
[13] Zhang X, Huang YQ, Liu XY, Yang L, Shi CD, Wu YC, et al. Microstructures and properties of 40Cu/Ag(invar) composites fabricated by powder metallurgy and subsequent thermo-mechanical treatment. Metall Mater Trans 2018;49A:1869–78. https://doi.org/10.1007/s11661-018-4548-9.
[14] Jha S. CUVAR®-a new controlled expansion, high conductivity material for electronic thermal management. In: 1995 proceedings. 45th electronic components and Technology conference; 1995 May 21-24. p. 542–7. https://doi.org/10.1109/ECTC.1995.515336. Las Vegas, NV, USA.
[15] Jha SC, Forster JA, Breit HF. Circuit system, a composite material for use therein, and a method of making the material. https://ppubs.uspto.gov/dirsearch-public/print/downloadBasicPdf/5310520?requestToken=eyJzdWIiOiI1N2ZlZjMyZi1iMTI2LTQwMzctYWYwYS0zZjM3MmFjNjYyNmUiLCJ2ZXIiOiIxYzQ1ODU2OC1mM2JhLTRhMmItODhlMy0zMmZmNTVhZTU5NmUiLCJleHAiOjB9; 1994.
[16] Yin S, Cavaliere P, Aldwell B, Jenkins R, Liao HL, Li WY, et al. Cold spray additive manufacturing and repair: fundamentals and applications. Addit Manuf 2018;21:628–50. https://doi.org/10.1016/j.addma.2018.04.017.
[17] Moridi A, Hassani-Gangaraj SM, Guagliano M, Dao M. Cold spray coating: review of material systems and future perspectives. Surf Eng 2014;30:369–95. https://doi.org/10.1179/1743294414y.0000000270.
[18] Assadi H, Kreye H, Gärtner F, Klassen T. Cold spraying - a materials perspective. Acta Mater 2016;116:382–407. https://doi.org/10.1016/j.actamat.2016.06.034.
[19] Cao K, Yu M, Liang CM, Chen H. Study on thermal conductivity of cold sprayed Cu coating. Surf Eng 2020;36:1058–66. https://doi.org/10.1080/02670844.2020.1790170.
[20] Chen CY, Xie YC, Liu LT, Zhao RX, Jin XL, Li SQ, et al. Cold spray additive manufacturing of Invar 36 alloy: microstructure, thermal expansion and mechanical properties. J Mater Sci Technol 2021;72:39–51. https://doi.org/10.1016/j.jmst.2020.07.038.
[21] Schmidt T, Assadi H, Gärtner F, Richter H, Stoltenhoff T, Kreye H, et al. From particle acceleration to impact and bonding in cold spraying. J Therm Spray Technol 2009;18:794–808. https://doi.org/10.1007/s11666-009-9357-7.
[22] Xiong YM, Xiong X, Yoon S, Bae G, Lee C. Dependence of bonding mechanisms of cold sprayed coatings on strain-rate-induced non-equilibrium phase transformation. J Therm Spray Technol 2011;20:860–5. https://doi.org/10.1007/s11666-011-9634-0.
[23] Hassani-Gangaraj M, Veysset D, Nelson KA, Schuh CA. In-situ observations of single micro-particle impact bonding. Scripta Mater 2018;145:9–13. https://doi.org/10.1016/j.scriptamat.2017.09.042.
[24] Maire E, Withers PJ. Quantitative X-ray tomography. Int Mater Rev 2014;59:1–43. https://doi.org/10.1179/1743280413y.0000000023.
[25] Kul M, Akgul B, Karabay YZ. The relationship of hot and cold rolling processes with the structure and properties of invar 36. Mater Chem Phys 2023;295. https://doi.org/10.1016/j.matchemphys.2022.127215.
[26] Bielousova O, Kocimski J, Maev RG, Smurov I, Scharff W, Leshchynsky V. Localisation of deformation in cold gas dynamic spraying. Surf Eng 2016;32:655–62. https://doi.org/10.1179/1743294415y.0000000059.
[27] Schmidt T, Gärtner F, Assadi H, Kreye H. Development of a generalized parameter window for cold spray deposition. Acta Mater 2006;54:729–42. https://doi.org/10.1016/j.actamat.2005.10.005.
[28] Wei FJ, Chou BY, Fung KZ, Tsai SY. Thermomechanical properties of cold-sprayed copper coatings from differently fabricated powders. Surf Coating Technol 2022;434:128128. https://doi.org/10.1016/j.surfcoat.2022.128128.
[29] Gärtner F, Stoltenhoff T, Voyer J, Kreye H, Riekehr S, Koçak M. Mechanical properties of cold-sprayed and thermally sprayed copper coatings. Surf Coating Technol 2006;200:6770–82. https://doi.org/10.1016/j.surfcoat.2005.10.007.
[30] Huang R, Sone M, Ma W, Fukanuma H. The effects of heat treatment on the mechanical properties of cold-sprayed coatings. Surf Coating Technol 2015;261:278–88. https://doi.org/10.1016/j.surfcoat.2014.11.017.
[31] Turner PS. Thermal-expansion stresses in reinforced plastic. J Res Natl Bur Stand 1946;37:239–50. https://doi.org/10.6028/jres.037.015.
[32] Schapery R. Thermal expansion coefficients of composite materials based on energy principles. J Compos Mater 1968;2:380. https://doi.org/10.1177/002199836800200308.
[33] Rosen B, Hashin Z. Effective thermal expansion coefficients and specific heats of composite materials. Int J Eng Sci 1970;8:157. https://doi.org/10.1016/0020-7225(70)90066-2.
[34] Fahmy A, Ragai A. Thermal-expansion behavior of two-phase solids. J Appl Phys 1970;41:5108–11. https://doi.org/10.1063/1.1658619.
[35] Hasselman DPH, Johnson LF. Effective thermal-conductivity of composites with interfacial thermal barrier resistance. J Compos Mater 1987;21:508–15. https://doi.org/10.1177/002199838702100602.
[36] Maxwell J. A treatise on electricity and magnetism. Nature 1873;7:478–80. https://doi.org/10.1038/007478a0.
[37] Benveniste Y. Effective thermal-conductivity of composites with a thermal contact resistance between the constituents-nondilute case. J Appl Phys 1987;61:2840–3. https://doi.org/10.1063/1.337877.
[38] Every A, Tzou Y, Hasselman D, Raj R. The effect of particle-size on the thermal-conductivity of zns/diamond composites. Acta Mater 1992;40:123–9. https://doi.org/10.1016/0956-7151(92)90205-s.
[39] Khan SA, Ziya AB, Ibrahim A, Atiq S, Ahmad N, Bashir F. The enhanced range of temperature for coefficient of low thermal expansion, electrical and thermal conductivities of Cu substituted Fe-Ni invar alloys. Phys Scripta 2016;91. https://doi.org/10.1088/0031-8949/91/3/035701.
[40] Liu XJ, He ZF, Shi Z, Yang SY, Wang CP. Investigation on the microstructures and thermal expansion characteristic of Cu-$Fe_{64}Ni_{36}$ alloys. J Xiamen Univ 2014;53:538–43. https://doi.org/10.6043/j.issn.0438-0479.2014.04.018.
[41] Schubert T, Brendel A, Schmid K, Koeck T, Ciupiński Ł, Zieliński W, et al. Interfacial design of Cu/SiC composites prepared by powder metallurgy for heat sink applications. Compos Appl Sci Manuf 2007;38:2398–403. https://doi.org/10.1016/j.compositesa.2007.08.012.
[42] Wang B, Yang F, Zhang H, He P. Microstructure and interface evolution of diamond/Cu composites prepared via ultrasonic additive manufacturing (UAM). J Mater Res Technol 2023;25:546–51. https://doi.org/10.1016/j.jmrt.2023.05.191.
[43] Ouyang M, Xu L, Zhang Q, Wang C, Wang C, Zhang H, et al. Effects of jet milling on W–10wt.%Cu composite powder for injection molding. J Mater Res Technol 2020;9:8535–43. https://doi.org/10.1016/j.jmrt.2020.05.107.
[44] Wei Y, Xie Z-R, Wu X-J, Liu T, Li Z-D. Effect of Mo content on interfacial microstructure and properties of explosive welded Mo–Cu/Cu plates. J Mater Res Technol 2023;27:2806–13. https://doi.org/10.1016/j.jmrt.2023.10.097.